Nuclear Engineering and Design 141 (1993) 69–82
North-Holland

Numerical analysis of bubble motion with the VOF method

Akio Tomiyama [a], Iztok Zun [b], Akira Sou [a] and Tadashi Sakaguchi [a]

[a] *Faculty of Engineering, Kobe University, Rokkodai, Nada Kobe 657, Japan*
[b] *Faculty of Mechanical Engineering, University of Ljubljana, Murnikova 2, 61000 Ljubljana, Slovenia*

Received 1 October 1992

Numerical analyses of a two-dimensional single bubble in a stagnant liquid and in a linear shear flow were conducted in the present study using the volume of fluid method, which is based on the local-instantaneous field equations. It was clarified that this method gives qualitatively appropriate predictions for the effects of the Morton number and the Eotvos number on fluctuating bubble motion in a stagnant liquid. Calculated velocity and pressure distributions indicated that the Karman vortex causes a sinuous movement of the bubble. As for the bubble motion in a linear shear flow, calculated bubbles migrated in a lateral direction. The direction of the lateral migration agreed to available experimental data. It was also confirmed that (i) the direction or the magnitude of the lateral migration is affected by the Eotvos and the Morton numbers, and (ii) the interaction among the internal flow of the bubble, the wake of the bubble and the external shear flow plays an essential role for the lateral migration.

1. Introduction

Sufficient knowledge on bubble motion in a dispersed gas–liquid two-phase flow is indispensable for establishing a reliable mathematical model to describe the flow dynamics. The behavior of bubbles moving in a liquid differs from that of solid particles in two main aspects: (i) the bubble is deformed under the action of hydrodynamic force, and (ii) an internal circulation may ensue due to momentum transfer across the gas–liquid interface [1]. In spite of a number of publications, our understanding on bubble motion is still rather rudimentary. Complex phenomena induced by interfacial interactions such as flow separation and wake configuration are examples which call upon the explanations from the first principles. On the other hand, for engineering purposes, a great deal of works have been carried out to obtain empirical correlations based on dimensionless groups. Grace [2], [3], for example, summarized available experimental data and deduced a well-known graphical correlation on shapes and terminal velocities of a single rising bubble in an infinite stagnant liquid. This correlation demonstrated that two dimensionless numbers, i.e., the Eotvos number and the Morton number, determine characteristics of bubble motion under a gravitational field. White and Beardmore [4] proposed a similar graphical correlation for terminal rising velocity of a Taylor bubble in a stagnant liquid confined in a vertical round tube. Their correlation also indicated the importance of the two aforementioned dimensionless numbers. These early works imply that complex fluctuating bubble motion is also strongly affected by the Eotvos and the Morton numbers. However no attempts have been made to clarify the relations between these two numbers and bubble motion. Up to the present, most attention has been paid only to the relation between the bubble diameter and the fluctuating bubble motion [5], [6].

In addition to bubble motion in a stagnant liquid, it is necessary to clarify the effect of liquid velocity distribution on bubble motion in order to develop a mathematical model for bubbly two-phase flow. Kariyazaki [7] conducted a fundamental experiment to investigate bubble behavior in a linear shear liquid flow. He found that the bubble is apt to migrate toward a higher velocity region while it deforms from spherical shape to wing shape. On the other hand, Sekoguchi et al. [8] observed behavior of a single bubble in an upward flow in a rectangular duct. They reported that small bubbles tend to rise near the wall of the duct, and large bubbles are apt to migrate to the center of the duct. Based on these experimental data, it was guessed by Serizawa and Kataoka [9] that complex vortices generated by a bubble may affect bubble behavior in a liquid flow. However this effect has not been confirmed yet. On the other hand, there were some efforts spent to

study the coupling of bubble intrinsic periodic movement and the bulk liquid shear field by Zun [10]. It has been shown in this work that only the bubbles having non-rectilinear intrinsic movement, which is basically periodic structure, are attracted by the channel walls in a cocurrent upward flow.

Recent rapid progress in computer power and in numerical methods gives us a large possibility for simulating complex bubble motion directly. That is to say, if we can solve the local-instantaneous field equations for gas and liquid phases together with appropriate jump conditions at the gas-liquid interface, the mechanism of complex bubble motion will be clarified in principle. One of the numerical methods which may enable us this kind of simulation is the volume of fluid (VOF) method proposed by Hirt and Nichols [11], [12]. However, the VOF method had not been applied to the analyses of bubble motion. Hence the authors [13], [14] examined the applicability of the VOF method to the analyses of a single rising bubble in an infinite stagnant liquid. This examination confirmed that the VOF method can give good prediction concerning the effects of the Morton and the Eotvos numbers on bubble shape and terminal velocity. Fluctuating bubble motion was not examined yet since the analyses were conducted using two-dimensional cylindrical coordinates. Then, in order to check if the VOF method can predict the effect of a channel wall on bubble shapes and terminal velocities, the authors [15], [16] recently applied this method to a Taylor bubble. The terminal velocity of the Taylor bubble predicted by this method agreed to White and Beardmore's correlation under a wide range of the Eotvos and the Morton numbers. Calculated bubble shapes also agreed well to ones measured by the authors. A brief review on these examinations will be described in this report.

Fluctuating bubble motion under a laminar flow condition was analyzed with the VOF method in the present study in order to check if this method can simulate such phenomena well. Since three-dimensional analyses require enormous CPU time even with an existing supercomputer, the present analyses were conducted for a two-dimensional bubble. In order to realize a numerical simulation of bubbly two-phase flow based on the local-instantaneous equations, a numerical method must possess the ability to predict the effect of liquid velocity field on bubble behavior. Hence, bubble motion in a linear shear flow was also

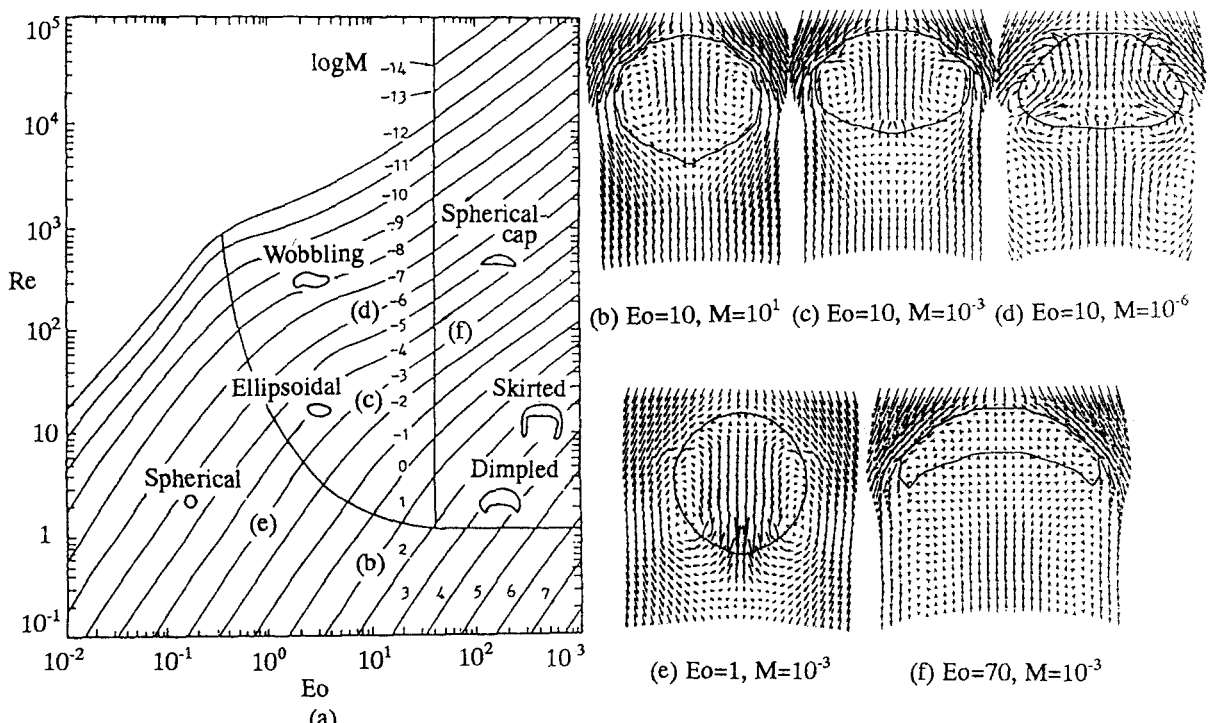

Fig. 1. (a) Grace's graphical correlation [2], [3]; (b)–(f) calculated bubble shapes and velocity distributions [13], [14]. (a, left) $Eo_D = 3.3$, (b, middle) $Eo_D = 13.3$, (c, right) $Eo_D = 30.0$.

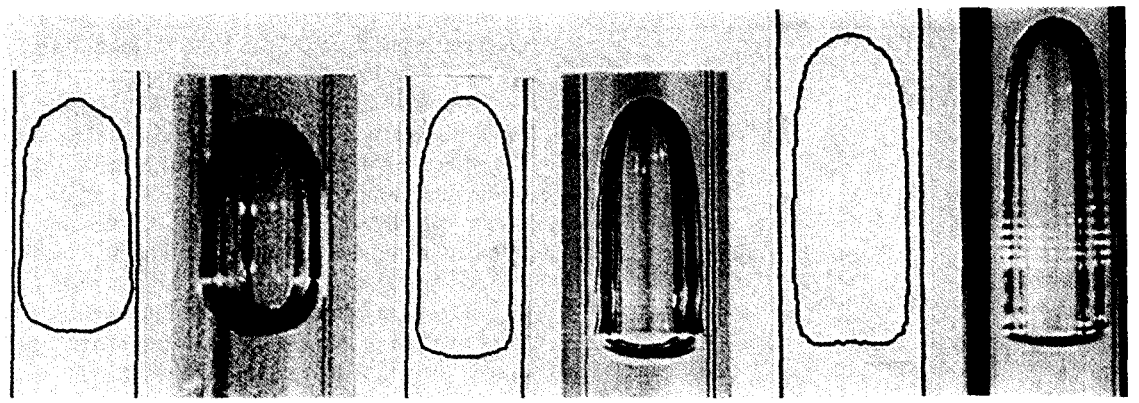

Fig. 2. Comparison between measured and calculated Taylor bubble shapes [15], [16]. (a, left) $Eo_D = 3.3$, (b, middle) $Eo_D = 13.3$, (c, right) $Eo_D = 30.0$.

analyzed with the VOF method. Calculated results were compared qualitatively with available experimental data.

2. Brief review on preliminary studies

An outline of the VOF method [11], [12] and some preliminary studies carried out by the authors [13]–[16] are briefly described here to show that this method can predict shapes and corresponding terminal velocities reasonably well.

2.1. Outline of the VOF method

The local-instantaneous mass and momentum equations solved by the VOF method are given by

$$\text{div } \boldsymbol{V}_k = 0, \tag{1}$$

$$\frac{D\boldsymbol{V}_k}{Dt} = -\frac{1}{\rho}\,\text{grad } p + \boldsymbol{g} + \nu_k \,\text{div grad } \boldsymbol{V}_k, \tag{2}$$

where the subscript k denotes the phase index (k = G or L for gas or liquid phase, respectively), $\boldsymbol{V}$ the velocity vector, p the pressure, $\boldsymbol{g}$ the body force per unit mass, ν the kinematic viscosity, ρ the density, t the time, and D/Dt is the substantial derivative. The density ρ in eq. (2) is defined by

$$\rho = (1-F)\rho_G - F\rho_L, \tag{3}$$

where F denotes the volume fraction of the liquid phase in a computational cell. Since F corresponds to the cell-averaged liquid volumetric fraction, the gas–liquid interface exists in a cell whose value of F lies between 0 and 1. The location and the curvature κ of the interface are determined by using the values of F in the eight cells surrounding the interface cell. An additional pressure, p_s, due to surface tension σ is calculated by

$$p_s = \kappa\sigma. \tag{4}$$

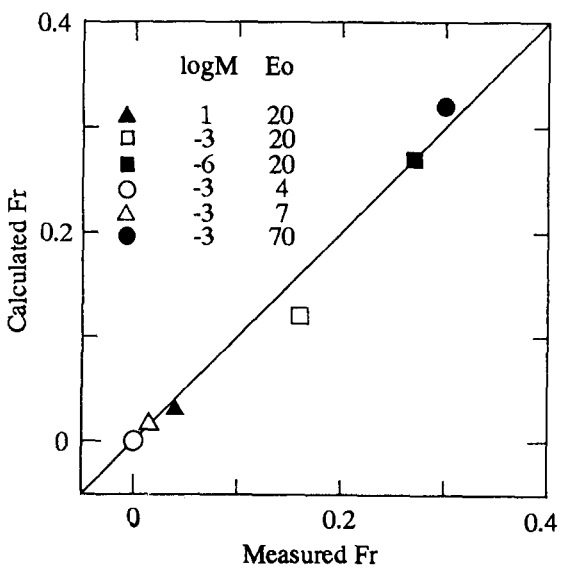

Fig. 3. Comparison between measured [4] and calculated Froude number Fr; $Fr = V_t/\sqrt{gD(\rho_L - \rho_G)/\rho_L}$.

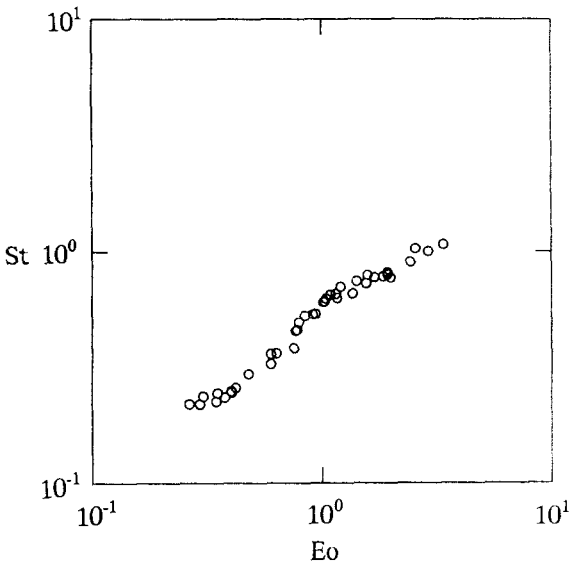

Fig. 4. The effect of Eo on St obtained from Zun's experimental data [5].

The force due to the above pressure is added to the right-hand side of eq. (2) to include the effect of the surface tension on velocity and pressure fields in the advanced time.

Since F moves with the fluid, F is governed by

$$\frac{DF}{Dt} = 0. \tag{5}$$

The above equation is solved numerically to advance the interface location.

As mentioned above, only the effect of the surface tension is taken into account at the gas–liquid interface. Furthermore, eq. (2) is solved by using the mixture density at the interface cell. In a sence, this means that the two fluids in the interface cell are treated as a homogeneous fluid concerning the momentum balance. It should be also noted that the interface velocity is not defined in the VOF method but calculated by interpolating the velocities in the neighborhood of the interface, which means that we cannot specify any boundary condition on interface slip induced by entropy generation [17]. Consequently, we cannot expect to obtain solutions which satisfy the jump condition exactly at the gas–liquid interface [17]. Nevertheless, it was confirmed by the authors [13]–[16] that the VOF method can give good predictions for terminal velocities and bubble shapes as described below.

2.2. Applicability of the VOF method to bubble analyses

In the previous reports [13]–[16], the authors examined the applicability of the VOF method to the analyses of single bubble motion. Firstly, a single bubble rising through an infinite stagnant liquid was analyzed to check whether the VOF method could predict well the effects of fluid properties and a bubble diameter on bubble motion. For this purpose, comparisons between calculated and measured bubble shapes and terminal rising velocities were conducted by utilizing Grace's graphical correlation [2], [3] shown in fig. 1(a). This graphical correlation takes into account the effects of fluid properties and an equivalent bubble diameter on the bubble shape and the terminal velocity using the following three dimensionless numbers:

$$M = \frac{g\mu_L^4(\rho_L - \rho_G)}{\rho_L^2\sigma^3}, \tag{6}$$

$$\mathrm{Eo} = g(\rho_L - \rho_G)d^2/\sigma, \tag{7}$$

$$\mathrm{Re} = V_t d/\nu_L, \tag{8}$$

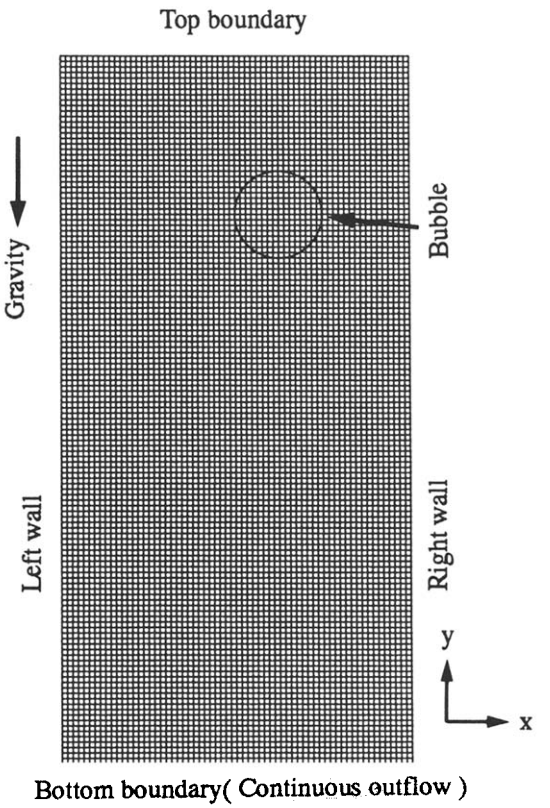

Fig. 5. Computational geometry.

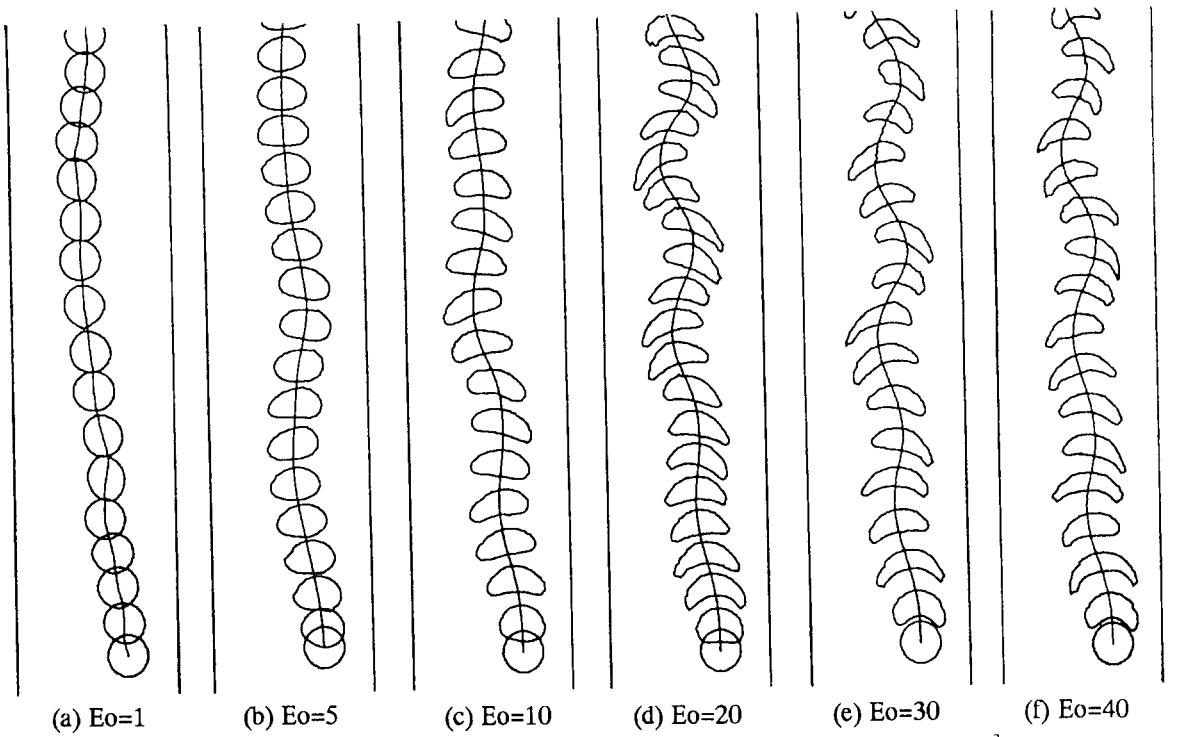

Fig. 6. Calculated results on the effect of Eo on fluctuating bubble motion under $M = 10^{-3}$.

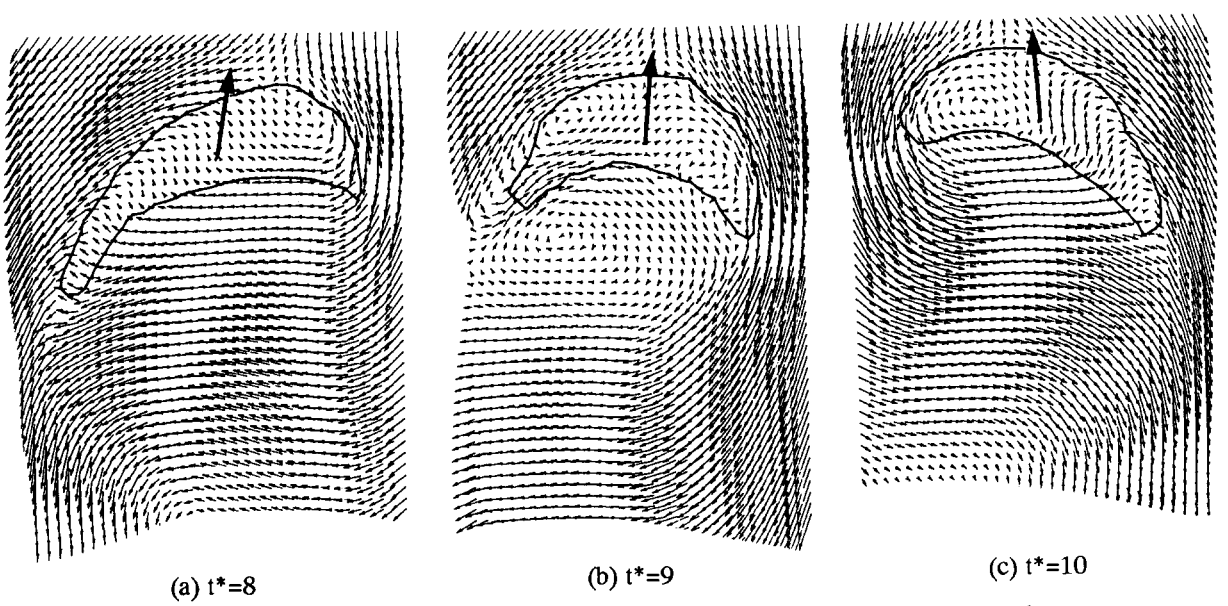

Fig. 7. Variation of velocity distribution with a dimentionless time t^* defined by $t^* = tV_t / d$; $M = 10^{-3}$ and Eo = 30.

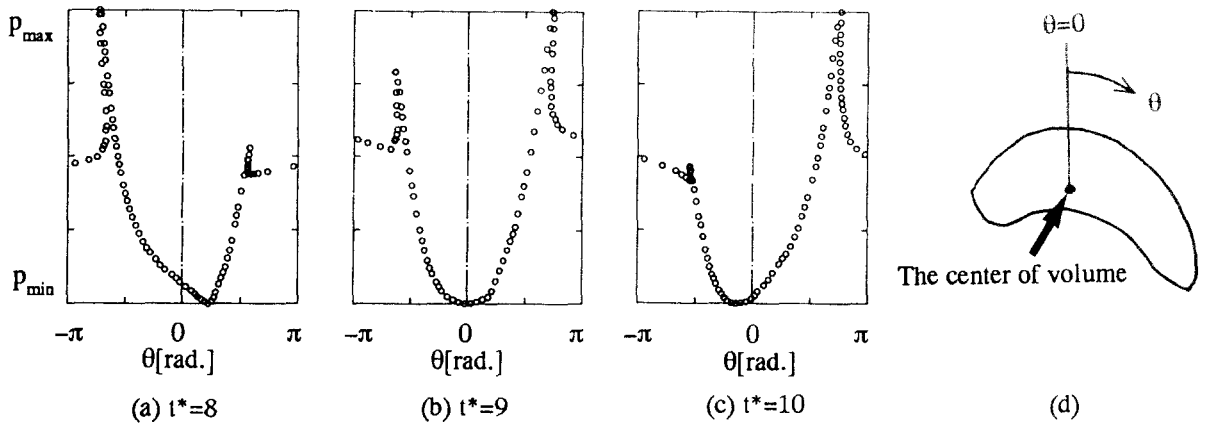

Fig. 8. (a)–(c) Azimuthal pressure distributions at the gas–liquid interface; (d) definition of θ.

where g denotes the gravity constant, μ the viscosity, d the equivalent bubble diameter, σ the surface tension, V_t the terminal velocity, M the Morton number which accounts for the effect of the fluid properties. Eo the Eotvos number representing the effect of the surface tension and the body force, and Re denotes the bubble Reynolds number.

Figures 1(b)–(f) are typical bubble shapes calculated by using two-dimensional cylindrical coordinates. As shown in these figures, the VOF method could predict the effects of fluid properties and the bubble diameter on bubble shape well. These analyses clarified that a velocity component normal to the interface shown in Figs. 1(d) and (e) induces a deformation of bubble shape. Furthermore, calculated terminal velocities were in good agreement with Grace's correlation under a wide range of the Morton and the Eotvos numbers.

Since characteristics of a Taylor bubble are considered to be much affected by the existence of a pipe wall, the Taylor bubble in a vertical round tube was analyzed with the VOF method to examine if this method can predict the effect of a wall. Figure 2 shows measured and calculated bubble shapes in a stagnant liquid for $Eo_D = 3.3$, 13.3 and 30.0, where Eo_D is a Eotvos number for the Taylor bubble defined by using the pipe diameter D as follows:

$$Eo_D = \frac{g(\rho_L - \rho_G)D^2}{\sigma}. \tag{9}$$

Bubble shapes were predicted well as shown in this figure. If the terminal rising velocity of the Taylor bubble is much affected by the interface slip due to the entropy generation, we will not be able to obtain accurate predictions for the terminal velocity without correct inclusion of the jump condition into the VOF method. As shown in fig. 3, calculated terminal rising velocity expressed in terms of the Froude number agreed well to White and Beardmore's graphical correlation under a wide range of Eo_D and M. This result indicates that the interface slip has little effect on the flow field within the calculated conditions.

3. Effects of Eo and M on fluctuating bubble motion

One of the authors, Zun [5], investigated the effect of the bubble diameter on fluctuating bubble motion experimentally. He measured V_t, d, and frequencies of

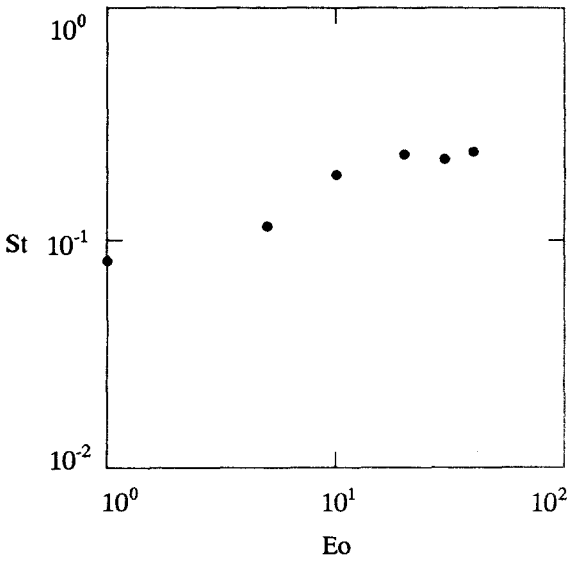

Fig. 9. Calculated Strouhal numbers.

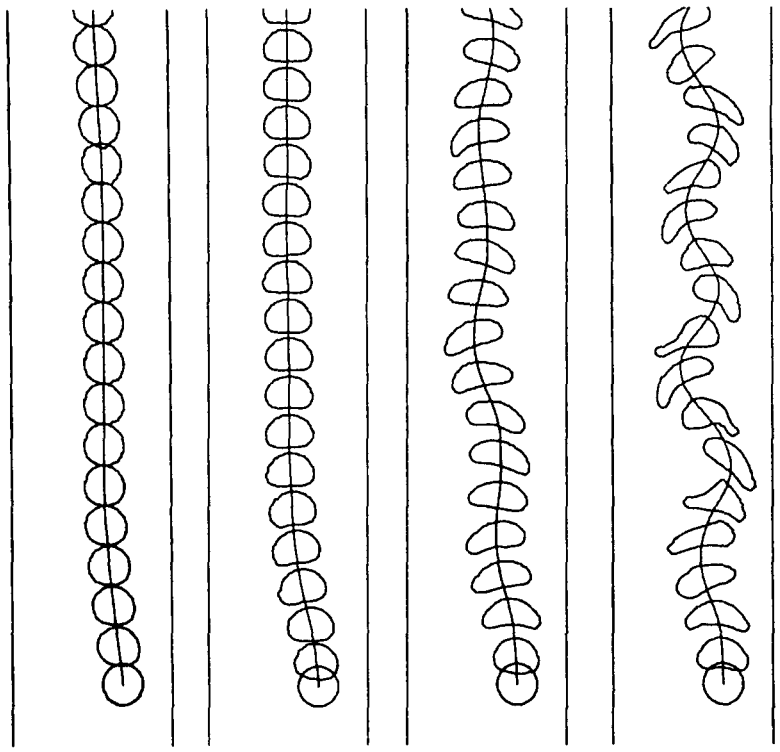

Fig. 10. Calculated results on the effect of M on fluctuating bubble motion under Eo = 10.

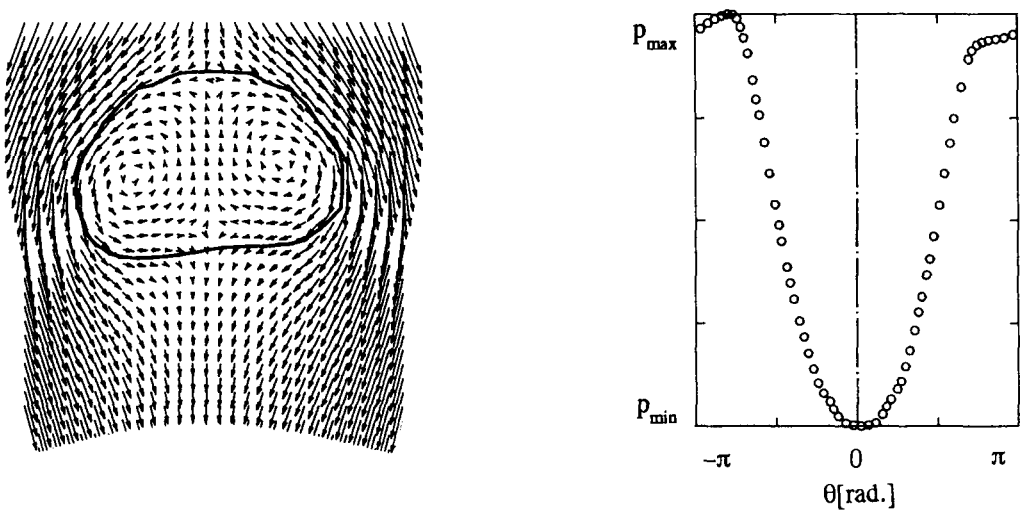

Fig. 11. Calculated velocity and pressure distribution for $M = 10^{-1}$ and Eo = 10.

periodic bubble motion, f. Since his experiments were conducted with filtered tap water and air at room temperature, we can assume that his experimental data were taken under a constant Morton number ($M = 10^{-11}$). Therefore, we can deduce a relation between Eo and the Strouhal number St defined by

$$\mathrm{St} = fd/V_t. \tag{10}$$

Figure 4 shows this relation. From this figure, we can see strong correlation between St and Eo, that is, all experimental data are on one curve. In this experimental range, St increases with Eo. The increasing rate of St, however, decreases gradually with increasing Eo. This may be because the bubble shape changes from wobbling to spherical-cap as Eo increases.

If the VOF method cannot predict the above-mentioned effects of the Eotvos number on fluctuating motion of a single rising bubble, we cannot expect it to give accurate prediction of bubbly two-phase flow. Hence, a numerical experiment was conducted to examine if it can give qualitatively appropriate relations between Eo and St. Since a three-dimensional analysis requires enormous CPU time even with an available supercomputer, the present analyses were conducted for a two-dimensional bubble in Cartesian coordinates. Figure 5 shows the computational mesh adopted in the analyses. The initial bubble shape was circle. Sixteen cells were assigned to the bubble diameter. The validity of this number had been confirmed by the previous studies [13], [14]. The initial position of the bubble was between the wall and the center of the channel in order to obtain asymmetric flow fields with small CPU time. The ratio of the bubble diameter to the channel width was fixed to 0.25 for all the analyses. From the top boundary, a liquid was fed in the downward direction at a uniform velocity V_{in}. The value of V_{in} was adjusted to be nearly equal to a terminal rising velocity so that the bubble did not escape from the computational domain. The left and the right walls were also moved in the downward direction at V_{in} to simulate a single rising bubble in a stagnant liquid in parallel walls. That is, these boundary conditions enable us to observe the bubble motion in a stagnant liquid from the coordinates moving upward with the bubble.

From the position of the center of volume of the bubble ($x_c(t)$, $y_c(t)$) in the computational domain, the bubble position vector ($x_B(t)$, $y_B(t)$) in the coordinates fixed to the stagnant liquid was calculated by

$$x_B(t) = x_c(t), \tag{11}$$

and

$$y_B(t) = y_c(t) + |V_{in}|\,t. \tag{12}$$

The bubble velocity (V_{Bx}, V_{By}) was obtained by

$$(V_{Bx}, V_{By}) = (\mathrm{d}x_B/\mathrm{d}t, \mathrm{d}y_B/\mathrm{d}t). \tag{13}$$

The differential terms in the right-hand side of the above equation were evaluated numerically by the centered difference method. For precise comparison between Zun's experimental data and calculated results, the width of the channel should be much wider than the width shown in fig. 5. However, we could not afford to use a wider channel due to the limitation of the CPU time. Hence, only qualitative comparisons were conducted by using the computational domain shown in fig. 5. In addition, all calculations were conducted for $M > 10^{-6}$ because it was difficult to obtain a numerically stable solution when $M < 10^{-7}$.

Calculated bubble trajectories under $M = 10^{-3}$ are shown in figs. 6(a)–(f) together with bubble shapes. As shown in these figures, calculated bubble shapes

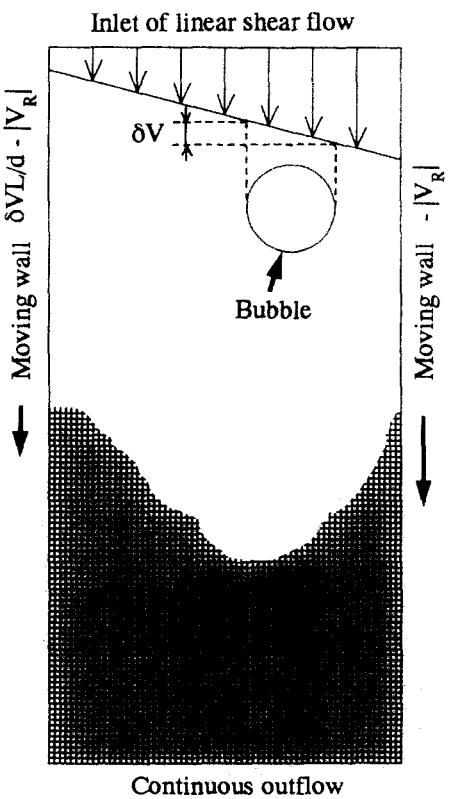

Fig. 12. Boundary conditions.

changed from spherical to spherical-cap as the Eotvos number increased. In the early stage of bubble motion, all bubbles migrated toward the center of the channel. This might be because the center of the channel is a stable position for the bubbles. Then, the bubbles began to move along more or less sinuous paths.

Figures 7(a)–(c) show a time history of velocity distribution around the fluctuating bubble when Eo is 30. The velocity distributions were plotted in the coordinates fixed at the upper end of the bubbles. We can see the Karman vortex shedding from the tail of the bubble. Figures 8(a)–(c) show the azimuthal pressure distribution at the gas–liquid interface. Each figure of fig. 8 corresponds to that of fig. 7. The origin of the azimuthal direction is shown in fig. 8(d). As shown in fig. 8, the azimuthal pressure distribution became asymmetric due to the vortex shedding. This asymmetric pressure distribution created a force to fluctuate

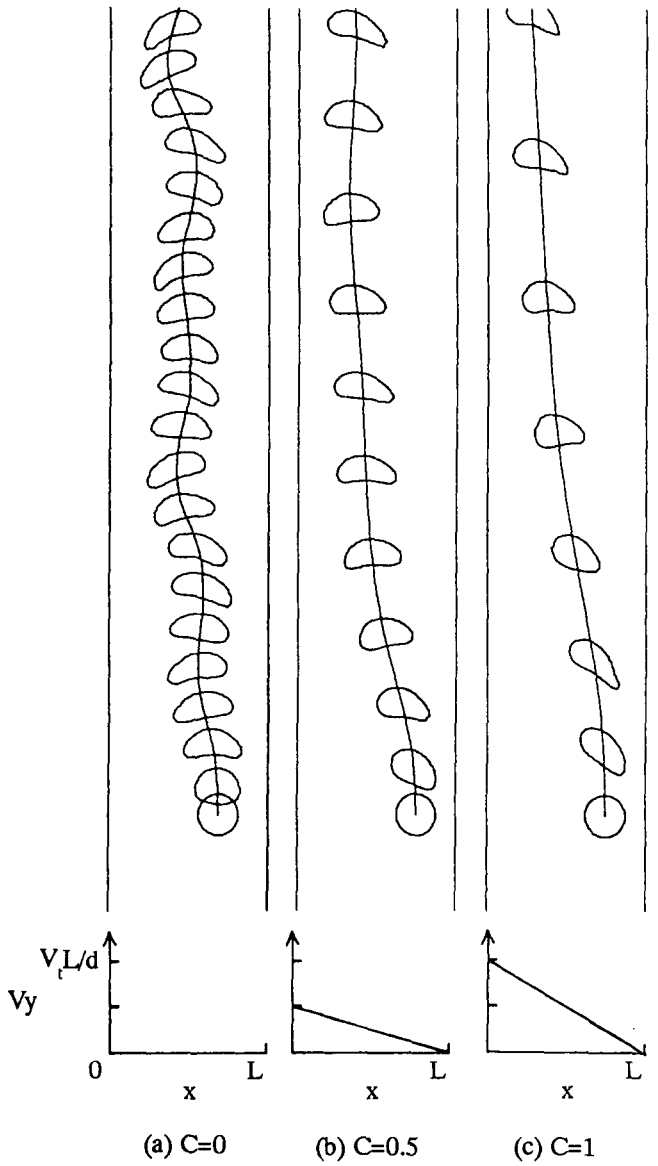

Fig. 13. Effect of a shear flow on bubble motion under Eo = 10 and $M = 10^{-3}$.

the bubble. The direction of the total pressure force acting on the bubble, which was deduced by integrating the azimuthal pressure, is shown by a bold arrow in figs. 7(a)–(c). We can judge the relation between the bubble shape and the direction of the total pressure force from these arrows.

From the wave length, λ, of the sinuous path, we can calculate St by

$$\mathrm{St} = d/\lambda. \tag{14}$$

The relation between calculated St and Eo is shown in fig. 9. The calculated St increased with Eo. The increasing rate became smaller as Eo increased. This tendency agrees with the experimental data shown in fig. 4.

Then, the effect of the Morton number was examined. Although there are few available experimental data on the relation between M and fluctuating bubble motion, we can guess this relation from Grace's graphical correlation shown in fig. 1(a). When Eo is around 10, fig. 1(a) indicates that the bubble shape changes from wobbling to ellipsoidal, and to spherical as M increases. This means that fluctuating motion will be weakened by increasing the Morton number. Calculated bubble shapes and their trajectories under Eo = 10 are shown in figs. 10(a)–(d). The fluctuation decreased with increasing the Morton number, which is consistent with Grace's graphical correlation. Moreover the fluctuation disappeared when $M = 10^{-1}$ and the bubble moved along a rectilinear path. In this case, symmetric creeping flow around the bubble was formed as shown in fig. 11(a). The azimuthal pressure distribution around the bubble was also symmetric as shown in fig. 11(b). This pressure distribution causes the rectilinear movement of the bubble.

Consequently, it was confirmed that the VOF method can give qualitatively good predictions for fluctuating bubble motion.

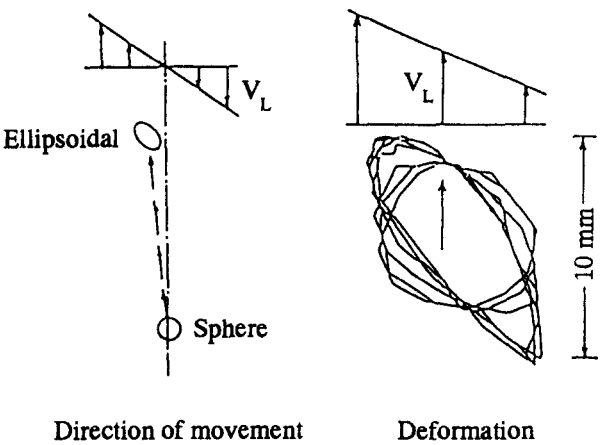

Fig. 14. Experimental data on bubble motion under a shear flow obtained by Kariyazaki [9].

4. Effect of liquid velocity distribution on bubble motion

In addition to the effects of M and Eo on a single rising bubble in a stagnant liquid, a numerical method, which is applicable to bubbly flow analyses, must possess the ability to predict the effect of the liquid velocity field on bubble motion accurately. Hence, numerical analyses of a single bubble in a linear shear flow were conducted. In these analyses, the magnitude of the velocity gradient of the shear flow was chosen as a parameter. Figure 12 shows boundary conditions adopted for the analyses. From the top boundary, a linear shear flow given by

$$V(x) = \frac{\delta V}{d}(L - x) - |V_R|, \quad (\delta V \geqq 0) \tag{15}$$

was fed in the downward direction. Here $\delta V/d$ denotes the magnitude of the velocity gradient, L the width of the channel and $|V_R|$ the modulus of the velocity at the right wall ($x = L$). Hence, the left and the right walls were moved at the velocities of $\delta VL/d - |V_R|$ and $-|V_R|$, respectively. The continuous outflow condition was imposed on the bottom boundary. The initial bubble size and shape, the number of the cells assigned to the bubble and the ratio d/L were identical with the analyses shown in the previous section. Therefore, if we set δV zero, we can obtain the same solutions as those obtained in the previous section. In order to examine the effect of the linear shear flow systematically, the value of δV was specified by referring to the terminal velocity in a stagnant liquid, V_t, which was obtained in the previous analyses. That is, δV was specified by

$$\delta V = CV_t, \tag{16}$$

where C is a parameter. Hence, $C = 0$ gives the same solution as the previous analyses, and $C = 1$ means that the value of the liquid velocity difference across the bubble is equal to the terminal rising velocity. The following analyses were conducted for $C = 0.5$ and $C = 1$. The value of $|V_R|$ was adjusted so as to keep the bubble in the computation domain. The bubble

position $(x_B(t), y_B(t))$ in the coordinates fixed to the right wall, i.e., the coordinates where the liquid velocity is zero at the right wall, was calculated by

$$x_B(t) = x_c(t), \tag{17}$$

and

$$y_B(t) = y_c(t) + |V_R|\, t. \tag{18}$$

Figure 13 shows calculated results for Eo = 10 and $M = 10^{-3}$. For $C = 0.5$ and 1, calculated bubbles migrated toward the higher velocity region. Kariyazaki [7] observed a deformation of a bubble in a linear shear flow. His result quoted from ref. [9] is shown in fig. 14. The direction of the lateral migration and the bubble deformation process shown in fig. 13 agreed really well with fig. 14. As for the fluctuating motion, the bubble moved along a slightly sinuous path when $C = 0.5$ as shown in fig. 13(b). On the other hand, the fluctuating motion was disappeared when $C = 1$. Hence, we can guess that intrinsic fluctuating motion of a bubble is suppressed by the high velocity gradient imposed on a bubble.

Then, bubble motion when Eo = 1 and $M = 10^{-3}$ was analyzed in order to examine the effect of the Eotvos number. If we consider that the fluid properties in this analysis are equal to those in the above analysis,

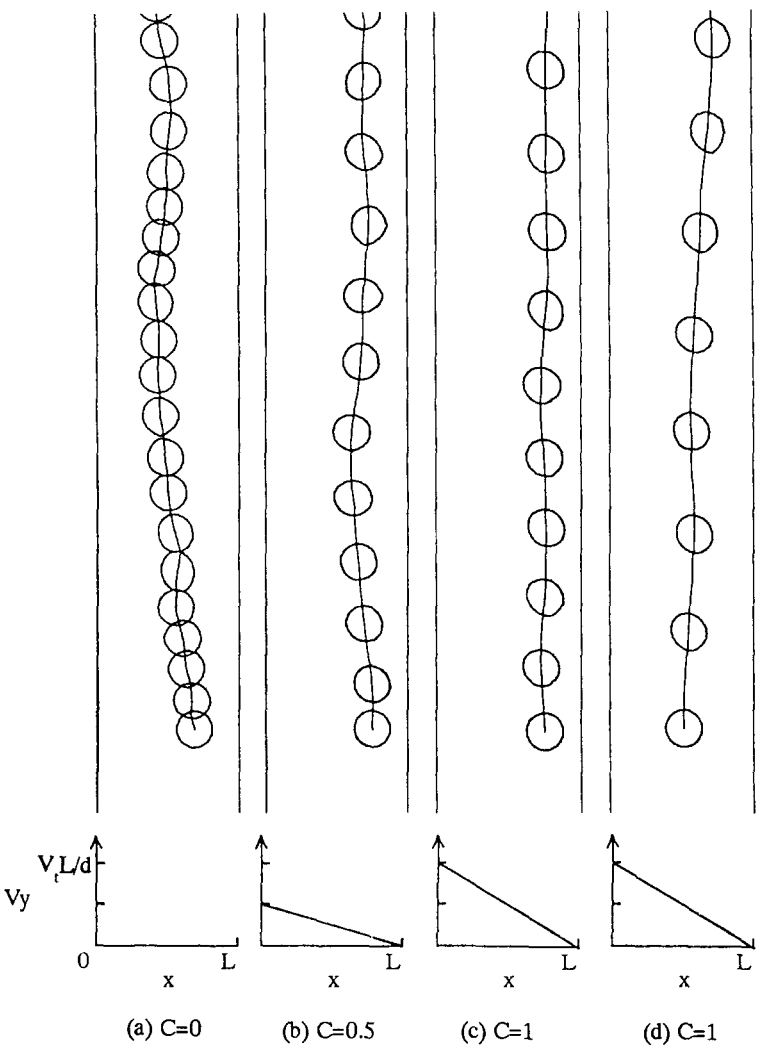

Fig. 15. Effect of a shear flow on bubble motion under Eo = 1 and $M = 10^{-3}$.

the bubble diameter in this analysis is considered to be smaller than that in the above analysis. Calculated results are shown in fig. 15. When C was 0, bubbles moved toward the center of the channel. However, when $C = 0.5$, horizontal position of the bubble did not change so much even after traveling a long vertical distance. Furthermore, when $C = 1$, the bubble slightly migrated toward the lower velocity region as shown in fig. 15(c). In order to make this opposite lateral migration more clear, another calculation was conducted by changing the initial bubble position to the center of the channel. The result of this additional calculation is shown in fig. 15(d). The lateral migration toward the lower velocity region is clearly observed in this figure. It has been recognized experimentally that small bubbles in a cocurrent two-phase bubbly upflow are apt to move near a pipe wall, which causes the so-called wall peak phase distribution. For example, Zun [10] observed that a small bubble whose diameter ranges from 0.6 mm to 5.1 mm travels toward the wall in the case of air–water two-phase bubbly flow. The bubbles shown in figs. 15(c) and (d) can be considered as a kind of bubbles which make the wall peak phase distribution.

Typical examples of velocity distributions for Eo = 1 and 10 are shown in fig. 16. We can see complex flow patterns, which are caused by the interaction among the internal flow of the bubble, the wake of the bubble and the external shear flow. As a result of this interaction, the total pressure force acting on the bubble directed to the lower velocity region when Eo = 1, or to the higher velocity region when Eo = 10. As for the direction of the lateral migration, Serizawa and Kataoka [9] supposed that a force to push the bubble to the lower velocity region will be induced by the interaction between the vortices generated by the bubble and the large velocity gradient due to turbulent flow. In the sense that the complex interaction determines the direction of the lateral migration, the present analyses support their presumption. However, the present analyses indicate that the turbulent flow is not necessarily required to change the direction of the lateral migration since the analyses were conducted under laminar flow conditions.

Then, the effect of the Morton number was examined. Figure 17 shows numerical solutions for Eo = 10 and $M = 10^{-1}$. By increasing the intensity of the velocity gradient, the bubble deformation to wing shape was dominated. This deformation resulted in the transverse migration toward the higher velocity region even though the speed of this migration was much slower compared with the bubble for Eo = 10 and $M = 10^{-3}$.

Consequently, it was confirmed that the effect of

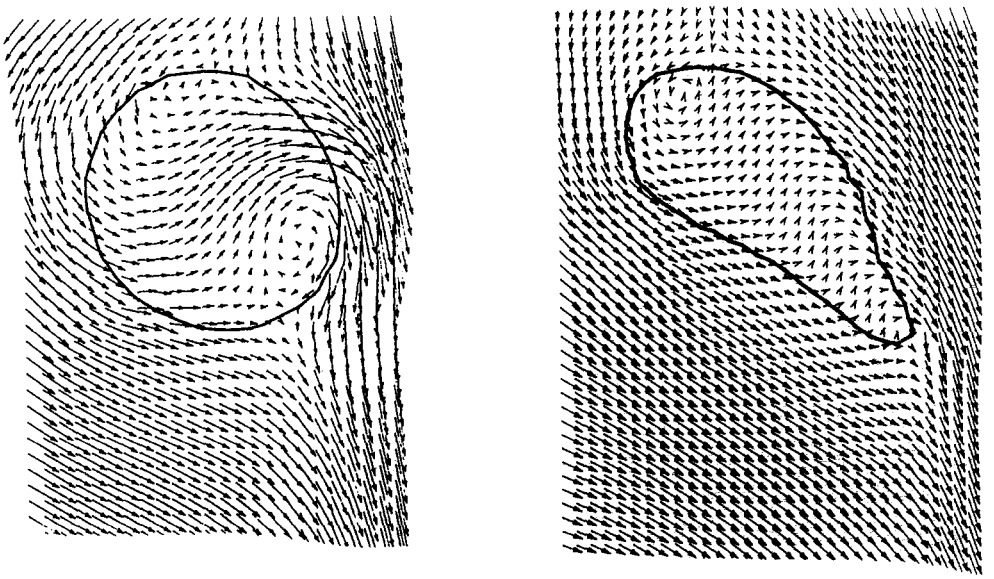

(a) Eo=1, M=10^{-3}, C=1 (b) Eo=10, M=10^{-3}, C=1

Fig. 16. Typical velocity distributions.

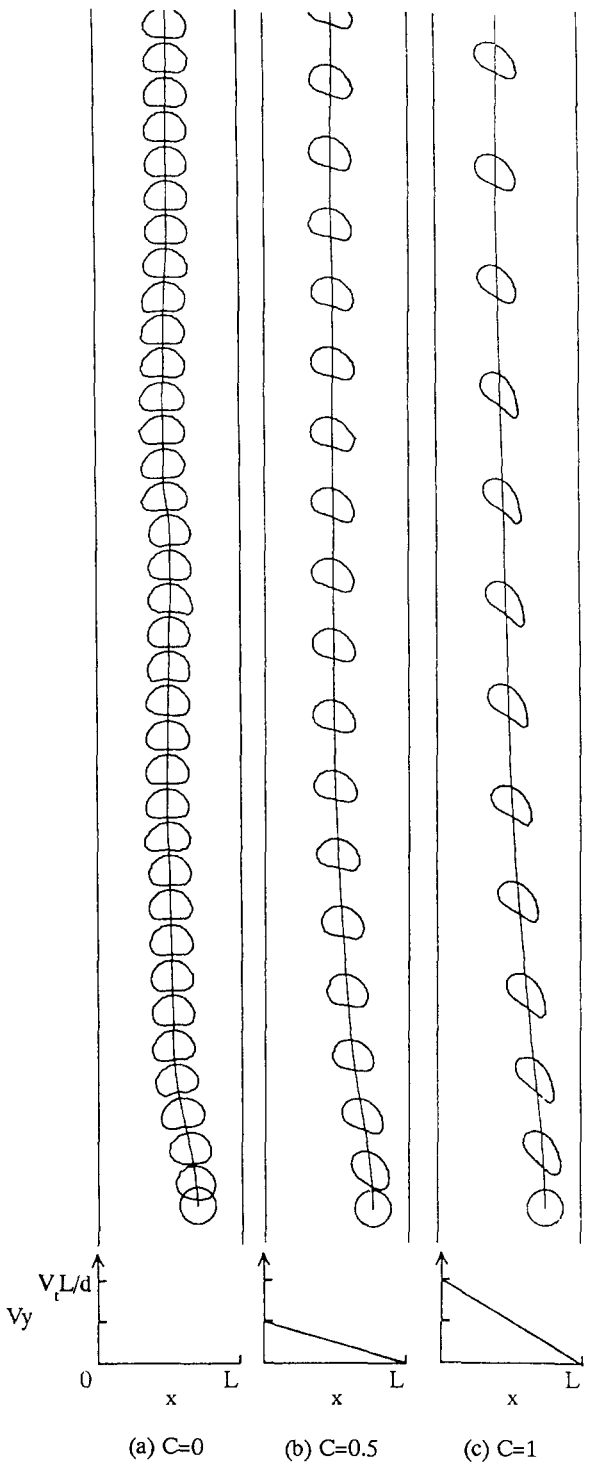

Fig. 17. Effect of a shear flow on bubble motion under Eo = 10 and $M = 10^{-1}$.

the liquid velocity field on the bubble motion can be predicted based on the local-instantaneous equations. Moreover, the present analyses indicate that the Eotvos number and the Morton number rather than the bubble diameter play an essential role on characteristics of the lateral migration of the bubble.

Further study should be conducted in the future to develop a numerical method which takes into account the jump condition exactly in order to obtain quantitatively accurate numerical solutions for bubble behavior.

5. Conclusions

In order to examine the possibility of detailed numerical analyses of two-phase bubbly flow, fluctuating motion of a two-dimensional bubble in a stagnant liquid and in a linear shear flow was analyzed numerically with the volume of fluid method. All analyses were conducted under laminar flow conditions. Since the bubble motion is known to be affected by the two dimensionless numbers, i.e., the Eotvos number and the Morton number, calculated results were compared with available experimental data by taking these dimensionless numbers as parameters. As a result, the following conclusions were obtained:

(1) As for the fluctuating bubble motion in a stagnant liquid, the VOF method could give qualitatively appropriate predictions for the effects of the Morton and the Eotvos numbers.

(2) The numerical analyses affirmed that the sinuous motion of the bubble is induced by the Karman vortex shedding from the tail of the bubble.

(3) The trajectories of the calculated bubbles in a linear shear flow agreed well with the available experimental data, that is, the transverse migration to the higher velocity region was obtained numerically when the Eotvos number was 10. On the other hand, when Eo = 1, the calculated bubble migrated toward the lower velocity region.

(4) It was confirmed that (i) the lateral migration can be induced by the interaction among the internal flow of the bubble, the wake of the bubble and the external shear flow, and (ii) the direction or the magnitude of the lateral migration is affected by the Eotvos and the Morton numbers.

Nomenclature

C parameter for adjusting the liquid velocity gradient,

d equivalent diameter of a bubble,
D pipe diameter,
Eo Eotvos number,
Eo_D Eotvos number for a Taylor bubble,
f frequency of periodical bubble motion,
F volume fraction of the liquid phase in a computational cell,
Fr Froude number,
g gravity constant,
$\boldsymbol{g}$ body force per unit mass,
L width of channel,
M Morton number,
p pressure,
Re Reynolds number,
St Strouhal number,
t time,
t^* dimensionless time defined by $V_t t/d$,
$\boldsymbol{V}$ velocity vector (V_x, V_y),
V_t terminal rising velocity,
V_R velocity of a right wall,
x horizontal coordinate,
y vertical coordinate.

Greek symbols

κ curvature of the interface,
λ wave length of sinuous bubble trajectory,
μ viscosity,
ν kinematic viscosity,
ρ density,
σ surface tension.

Subscripts

B bubble,
G gas phase,
k phase index,
L liquid phase.

References

[1] S. Winnikow and B.T. Chao, Droplet motion in purified systems, The Pysics of Fluid 9, 1 (1966) 50–61.
[2] J.R. Grace, Shapes and velocities of bubbles rising in infinite liquids, Trans. Inst. Chem. Eng. 51 (1973) 116–120.
[3] J.R. Grace, T. Wairegi, and T.H. Nguyen, Shapes and velocities of single drops and bubbles moving freely through immiscible liquids, Trans. Inst. Chem. Eng. 54 (1976) 167–173.
[4] E.T. White and R.H. Beardmore, The velocity of rise of single cylindrical air bubbles through liquids contained in vertical tubes, Chem. Engng. Sci. 17 (1962) 351–361.
[5] I. Zun, The non-rectilinear motion of bubbles rising through a stagnant and disturbed liquid, Proc. World Cong. III of Chem. Eng., Vol. II, Tokyo (1986) 214–217.
[6] H. Tsuge and S. Hibino, The motion of single gas bubbles rising in various liquids, Kagaku Kogaku, 35 (1962) 65–71 (in Japanese).
[7] A. Kariyazaki, Behavior of a gas bubble in a linear shear flow, Proc. 6th Two-Phase Flow Symposium of Japan (1985) 49–52, (in japanese).
[8] K. Sekoguchi, Y. Sato, and T. Honda, Two-phase bubble flow (First Report), Trans. Japan Soc. Mech. Engrs., 40–333 (1974) 1395–1403.
[9] A. Serizawa and I. Kataoka, Phase distribution in two-phase flow, ICHMT Int. Seminar on Transient Phenomena in Multiphase Flow, Dubrovnik, Yugoslavia, May (1987) 179–224.
[10] I. Zun, Transition from wall void peaking to core void peaking in turbulent bubbly flow, in: Transient Phenomena in Multiphase Flow, ed. N.H. Afgan (Hemisphere, Washington, D.C., 1988, 225–245.
[11] C.W. Hirt and B.D. Nichols, Volume of Fluid (VOF) method for the dynamics of free boundaries, J. Comput. Phys. 39 (1981) 201–225.
[12] B.D. Nichols, C.W. Hirt and R.S. Hotchkiss, SOLA-VOF: a solution algorithm for transient fluid flow with multiple free boundaries, LA-8355 (1980).
[13] A. Tomiyama, A. Sou, H. Minagawa, and T. Sakaguchi, Numerical analyses of a single bubble with VOF method, Trans. Japan Soc. Mech. Engrs. 57-539 (1991) 1–7 (in Japanese).
[14] A. Tomiyama, A. Sou, H. Minagawa, and T. Sakaguchi, Numerical analyses of a single bubble rising in liquids using the volume of fluid method, Proc. Int. Conf. on Multiphase Flows '91-Tsukuba, Vol. 1 (1991) 373–376.
[15] A. Tomiyama, A. Sou, M. Matsui, and T. Sakaguchi, Analyses of bubble behavior with the volume of fluid method, Proc. Fluids Eng. Conf. '91, JSME, No. 910-50 (1991) 341–343 (in Japanese).
[16] A. Sou, A. Tomiyama, and T. Sakaguchi, An examination on applicability of the VOF method to bubble analyses, Proc. 30th National Heat Transf. Symposium Japan (1992) (to be published in Japanese).
[17] J.M. Delhaye, Jump conditions and entropy sources in two-phase systems, local instant formulation, Int. J. Multiphase Flow 1 (1974) 395–409.